https://doi.org/10.46813/2025-156-122

STRUCTURE AND PHASE COMPOSITION OF ARC-PVD ZrTaN/ZrTiCuN NANOLAMINATE COATINGS

A.V. Taran[1], I.E. Garkusha[1,3], V.O. Stolbovyi[1,4], K. Nowakowska-Langier[2], S.P. Romaniuk[2]
[1]National Science Center "Kharkiv Institute of Physics and Technology", Kharkiv, Ukraine;
[2]National Centre for Nuclear Research, Otwock, Poland;
[3]V.N. Karazin Kharkiv National University, Kharkiv, Ukraine;
[4]Kharkiv National Automobile and Highway University, Kharkiv, Ukraine
E-mail: avtaran@ukr.net

In the present research the structure and phase composition of nanolaminate ARC-PVD ZrTaN/ZrTiCuN coatings have been investigated. Raman spectroscopy, scanning electron microscopy (SEM) with microanalysis (EDX), X-ray diffraction analysis were used to study the surface morphology, chemical composition and its distribution. The lattice parameters of the phases detected in the coatings by XRD differ from the literature values and the reason for such deviations can be both the presence of macrostrains in the coatings and the replacement of zirconium by other elements (Ta, Ti, Cu) in the sub-lattice cells of the above-mentioned phases.

PACS: 52.77.-j; 81.20.-n

INTRODUCTION

The monolayer coatings largely limit the properties and performance of hard coatings. The technology for nanometer-scale multilayered coatings also called superlattice, nanolaminate or nanocomposite could overcome this limit and create new materials, which might possess a combination of desired properties of its constituents or own enhanced properties better than its constituents [1].

Composite systems, such as nanolaminates and nanocomposite coatings, have been extensively studied to overcome the limitations of single films and achieve superior mechanical performance. During the last decades, the scientific and industrial interest towards the development of nanostructured multilayer coatings, i.e., nanolaminates, has remarkably grown [2]. Individual materials lack the complex array of properties required to provide effective protection towards wear sources. The fundamental benefit of using multilayer coatings lies specifically in the possibility to disentangle opposing materials properties, such as hardness and toughness, among the constituent materials. Synergistic effects arise when the thickness of the constituent layers falls in the nanometric regime including enhanced microhardness adhesion strength and corrosion resistance and slower wear rates.

A coating is formed consisting of nanolayers of evaporated metals or their nitrides, which alternate and necessarily differ in physical, technical or structural characteristics. Such coatings with layer periods from 10 to 300 nm while maintaining overall hardness can provide operability with a total thickness of up to 200 μm and above. The nanoscale nature of the layers makes it possible to reduce internal stresses and leads to the formation of new, previously unknown compositions with properties necessary for specific technological processes and conditions.

But such coatings definitely cannot be equally operable in different operating conditions. For example, coatings based on titanium nitride, by the way, are the cheapest, operate flawlessly on cutting tools when processing ordinary steel in the as-delivered state, achieving an increase in tool resistance up to 5–6 times, but are practically inoperable when processing ordinary chromium-nickel steels, in particular, stainless steel Kh18N10T [3]. When processing hardened steels, only multicomponent nanolayer coatings give positive results, but the elemental composition in different cathodes is different, which affects the operational properties [4]. For different materials subject to wear, it is necessary to develop the most optimal types of protective nitride coatings. This requires research into a number of nanolayer coatings with combinations of different nanostructured coatings in combination [5].

The selection of materials to be combined in such a multiphase structure should refer to their phase relations in the corresponding phase diagram. The resulting microstructure and property profile of a multiphase or nanocomposite coating is clearly determined by the plasma process parameters and by the kinetics of the deposition and growth process [6, 7].

In this research, polycrystalline nitride nanolaminates have been prepared with the right material combination and coating structures. The multilayer films were deposited by evaporation of two different target materials simultaneously in a multi-cathode vacuum-arc deposition system. The thickness of each layer was in the range of 70…80 nm and the total thickness of the multilayer is 3 μm. The structure and phase composition of nanolaminate PVD ZrTaN/ZrTiCuN coatings have been investigated.

1. EXPERIMENTAL SETUP

Coatings were applied in a modernized vacuum-arc installation "Bulat-6" (Fig. 1) using ZrTa and ZrTiCu alloyed cathodes as cathode materials. The "Bulat-6" vacuum-arc facility is also equipped with a source of constant voltage, the value of which can be changed in the range of -(5…1300) V, which is supplied to the substrate holder with samples.

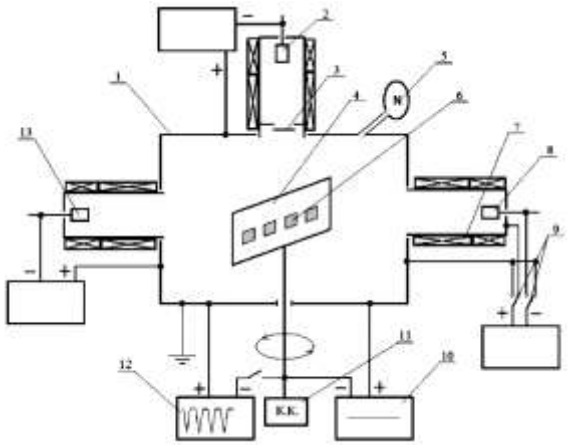

Fig. 1. Schematic diagram of a modernized vacuum-arc installation of the "Bulat-6" type for applying multilayer coating: 1 – vacuum chamber; 2 – vacuum-arc evaporator; 3 – metal screen; 4 – sample holder screen; 5 – nitrogen pressure regulator; 6 – samples; 7 – vacuum-arc evaporator body – gas discharge anode; 8 – ZrTa cathode; 9 – switching relay; 10 – constant voltage source; 11 – command controller; 12 – pulse voltage source; 13 – ZrTiCu cathode

For the ZrTa cathode evaporation, the arc discharge current was equal to 120 A, and for ZrTiCu it comprised 100 A. Polished stainless-steel of 12X18H9T type samples with dimensions of 20 × 20 × 3 mm as well as thin copper foils with a thickness of 0.2 mm were used as substrates to be coated. The substrates were previously washed in an alkaline solution using ultrasonic bath. The substrates were located at a distance of 250 mm from the evaporator. After the vacuum chamber was pumped down to a pressure of P = 0.006 Pa, a potential of -1300 V was applied to the substrates to provide cleaning and activation with ions of the cathode material for 9…10 min. Then metal layers were deposited at a pressure of P = 0.006 Pa and nitride layers at a nitrogen pressure of P = 0.26 Pa. A negative potential on the substrate comprised -200 V.

XRD examinations of the samples were carried out using DRON-UM1 X-ray diffractometer under copper Cu-Kα irradiation. The diffracted lines were recorded by a scintillation detector. Qualitative phase analysis of the samples was carried out using the ICDD PDF-2 international database of crystallographic compounds.

The study of the microstructural characteristics (the grain size and the level of microstrain) of the coatings was carried out by the integral width of the peaks using the Williamson-Hall method. The main formula (1) of the method is as following:

$$\beta = \frac{\lambda}{D \cdot \cos(\theta)} + 4 \cdot \varepsilon \cdot \mathrm{tg}(\theta)\,, \qquad (1)$$

where β is the true physical expansion; λ is the wavelength of X-ray irradiation; D – grain size; θ – diffraction angle; ε is the level of microstrain.

Structure and chemical composition of the coatings were investigated by scanning electron microscopy (SEM) and energy dispersive spectroscopy (EDS) by using ZEISS EVO® MA10. 3D surface morphology was also monitored by Keyence VK-X3000 series laser scanning microscope.

Specimens were also examined by using a confocal Raman microspectrometer by the WITec alpha 300R model manufactured by Oxford Instruments UK, equipped with a CCD camera. The specimens underwent excitation via a 532 nm Nd:YAG laser emitting 4 mW power. Raman spectra were recorded using a x100 lens within the spectral range of 70 to 3600 cm^{-1}, with an acquisition time of 80 s per spectrum, controlled by the Control 5.2 software. The initial data processing phase involved X-ray removal (XRR) and baseline correction, employing polynomial functions within the WITec Project FIVE 5.2 PLUS software. Subsequently, the spectra were exported for further analysis in OriginPro 9.9 software to generate the plots.

2. RESULTS AND DISCUSSION

Four phases were found in the coating according to XRD data (Fig. 2): two zirconium nitrides ZrN#1 and ZrN#2 and two modifications of pure zirconium Zr-α and Zr-β.

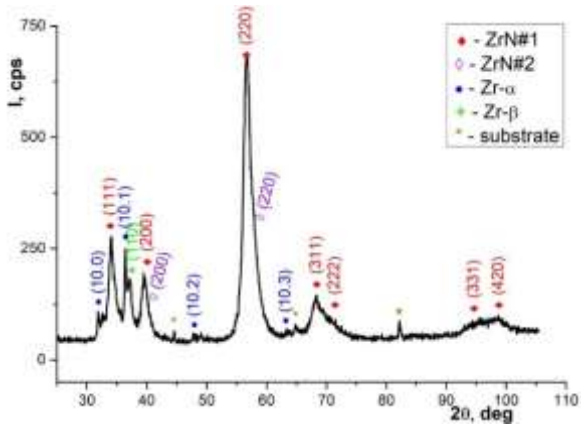

Fig. 2. XRD pattern from nanolayered ZrTaN/ZrTiCuN coating

The presence of two zirconium nitrides ZrN#1 and ZrN#2 is evidenced by the asymmetry of the peaks ("pulling" of the peaks towards larger 2θ angles). Presumably one nitride based on Zr and Ta (ZrN#1) and the other based on Zr, Ti, and Cu (ZrN#2). The intensity distribution of the diffraction peaks of both nitrides corresponds to a strong (220) texture. The lattice parameters of nitrides are a = 4.560 Å and a = 4.504 Å (for ZrN#1 and ZrN#2, respectively). The grain size for ZrN1 was 46.6 nm with the level of macrostrain $5.6 \cdot 10^{-3}$. The parameters of the Zr-α zirconium lattice are: a = 3.241 Å; c = 5.169 Å. The lattice parameter of zirconium Zr-β is a = 3.424 Å. It was not possible to estimate the microstructural characteristics for the detected phases (due to the significant overlap of the peaks, it is impossible to unambiguously determine their half-width, which is necessary for further calculations).

It should be noted that the lattice parameters of the phases detected in the coatings (ZrN, Zr-α, Zr-β) differ from the literature values (for ZrN: a = 4.574 Å; for Zr-α: a = 3.232 Å, c = 5.147 Å; for Zr-β: a = 3.545 Å). The reason for such deviations can be both the presence of macrostrains in the coatings and the replacement of zirconium by other elements (Ta, Ti, Cu) in the sub-lattice cells of the above-mentioned phases.

The Raman spectrum of the ZrTiCuN/ZrTaN sample shows that two bands appear in the spectral region below 300 cm^{-1}, occupying positions close to those observed in the ZrN spectrum from the literature (Fig. 3). Above 300 cm^{-1}, a broad band is observed, extending to approximately 700 cm^{-1}, although with reduced intensity in the sample. It is hypothesized that within the broad band centered around 532 cm^{-1} there may be a spectral feature that can be attributed to a non-stoichiometric CuN phase existence.

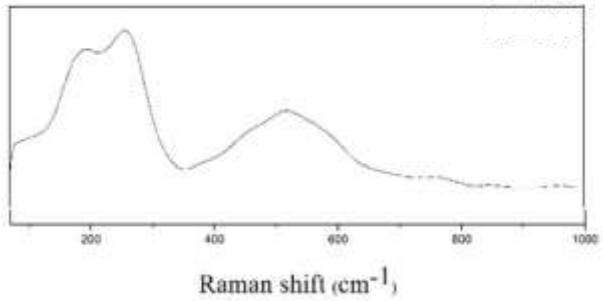

Fig. 3. Raman spectra from ZrTaN/ZrTiCuN coating

Figs. 4 and 5 depict SEM cross-section and EDS spectra from ZrTaN/ZrTiCuN coating, respectively. Nanolayered structure with alternating layers of 70…80 nm in thickness is clearly seen.

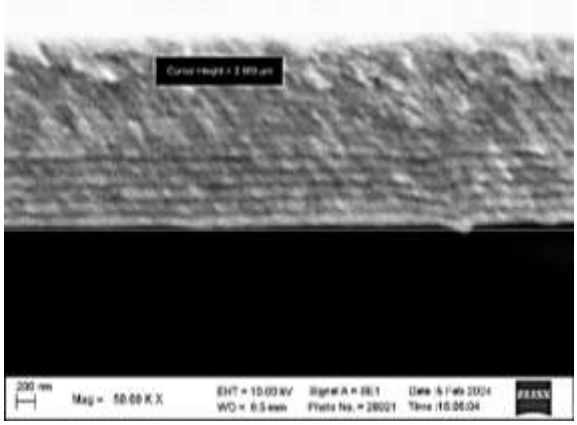

Fig. 4. SEM cross-section from ZrTaN/ZrTiCuN coating

It should be noted that the surface roughness in thin films is primarily due to the formation of structural and topographical defects during the deposition process [8, 9]. By replacing a continuous deposition with a stepwise deposition of alternating materials, the growth of such defects is reduced thanks to materials discontinuity and limited by the individual layers thickness.

Fig. 6 shows 3D surface morphology by Keyence VK-X3000 series laser scanning microscope and reveals a number of droplet related defects which are very common in the coatings deposited by cathodic arc deposition technique. If metal ions are used for substrate etching, then droplets generated by arc discharge contaminate the substrate surface, which cause the formation of growth defects.

While the generation of droplets continues also during deposition process the growth defects start to grow within the coating. The metal droplets are produced due to the melting of the target.

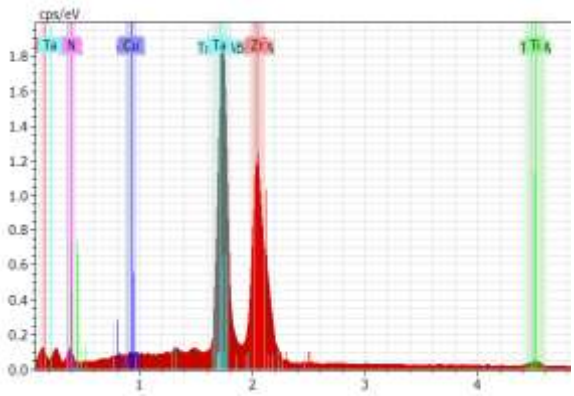

Fig. 5. EDS distribution of chemical elements

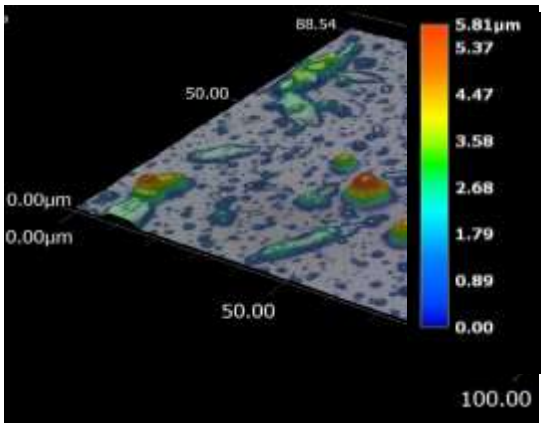

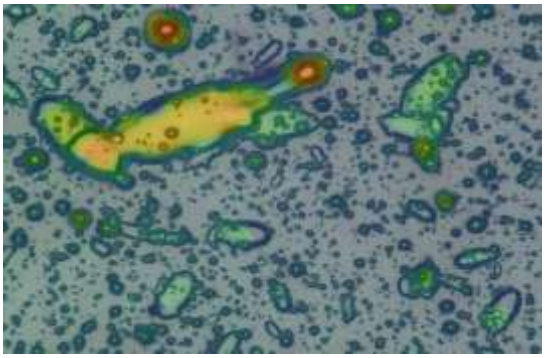

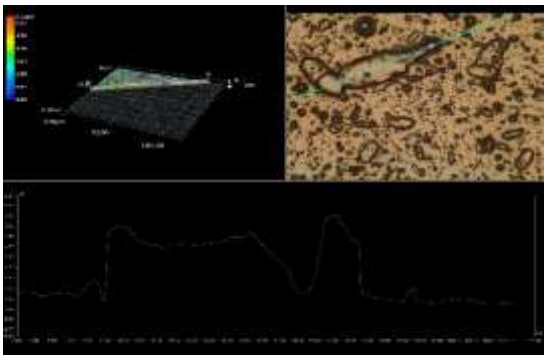

Fig. 6. 3D surface morphology by laser scanning microscope

The liquid target material is ejected from the target as droplets. Part of these droplets can arrive on the substrate surface where the liquid material solidifies. We speculate that such droplets originate mostly from copper and initiate defects in the depositing coatings. By using a scale in the right corner of the Fig. 6, it is very easy to estimate the size and height of such defects.

EDS mapping of distribution of chemical elements via the depth is shown in Fig. 7.

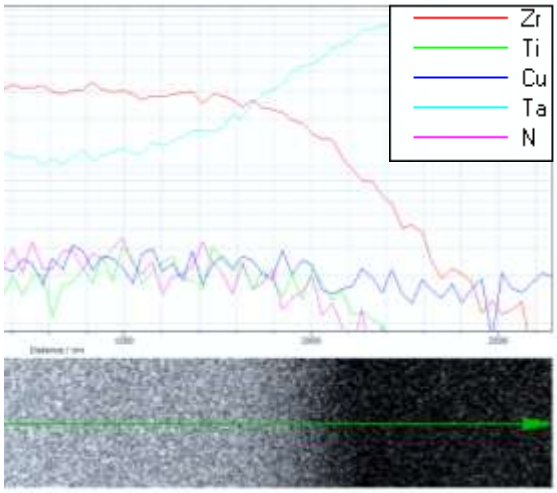

Fig. 7. EDS mapping of distribution of chemical elements via the depth

CONCLUSIONS

Polycrystalline nitride ZrTaN/ZrTiCuN nanolaminates have been deposited by evaporation of two different target materials simultaneously in a multi-cathode vacuum-arc deposition system. Nanolayered structure with alternating layers of 70…80 nm in thickness was grown. According to structural examinations the lattice parameters of the phases detected in the coatings (ZrN, Zr-α, Zr-β) differ from the literature values (for ZrN: a = 4.574 Å; for Zr-α: a = 3.232 Å, c = 5.147 Å; for Zr-β: a = 3.545 Å). The reason for such deviations can be both the presence of macrostrains in the coatings and the replacement of zirconium by other elements (Ta, Ti, Cu) in the sub-lattice cells of the above-mentioned phases. Raman spectroscopy revealed additional non-stoichiometric CuN phase formation.

ACKNOWLEDGEMENTS

Two members of the team of authors is grateful to the Simons Foundation Program: Presidential Discretionary-Ukraine Support Grants, Award № 1290591.

REFERENCES

1. A. Azizpour, R. Hahn, F.F. Klimashin, T. Wojci k, E. Poureidi. Deformation and cracking mechanism in CrN/TiN multilayer coatings // *Coatings.* 2019, v. 9 (363), p. 9-17.
2. R. Bendikiene, E. Pupelis. Application of surfaced cutters for machining of wood-based materials // *Wood Res*. 2016, v. 61(1), p. 155-162.
3. Y. Qiu. Improvement of tribological performance of CrN coating via multilayering with VN // *Surf. Coat. Technol.* 2013, v. 231, p. 357-363.
4. J.J. Roa, E. Jiménez-Piqué, R. Martínez, G. Ramírez, J.M. Tarragó, R. Rodríguez, L. Llanes. Contact damage and fracture micromechanisms of multilayered TiN/CrN coatings at micro- and nano-length scales // *Thin Solid Films*. 2014, v. 571 (P2), p. 308-315.
5. C. Gaona-Tiburcio, M. Montoya-Rangel, J.A. Cabral-Miramontes, F. Estupiñan-López, P. Zambrano-Robledo, R. Orozco Cruz, J.G. Chacón-Nava, M.Á. Baltazar-Zamora, F. Almeraya-Calderón. Corrosion resistance of multilayer coatings deposited by PVD on Inconel 718 using electrochemical impedance spectroscopy technique // *Coatings*. 2020, v. 10 (6), p. 1-11.
6. A.V. Taran, I.E. Garkusha, K. Nowakowska-Langier, G.N. Tolmachova, P.M. Vorontsov, O.A. Nikol'chenko, Yu.P. Gnidenko, S.P. Romaniuk, O.I. Tymoshenko, I.O. Misiruk. Microstructure, chemical composition, and nanomechanical properties of ARC-PVD ZrTa/$ZrTaO_2$ bilayer coatings // *Problems of Atomic Science and Technology*. 2024, N 4 (152), p. 132-135.
7. A.V. Taran, I.E. Garkusha, V.S. Taran, O.I. Tymoshenko, I.O. Misiruk, S.P. Romaniuk, T.V. Mal'tsev, V.V. Starikov. Zr O_2/ZrN multilayers on bare sintered NdFeB magnets by ion-plasma deposition with pulsed biasing // *High Temperature Material Processes*. 2020, v. 24(1), p. 9-20.
8. P. Panjan, A. Drnovšek, P. Gselman, M. Čekada, M. Panjan. Review of growth defects in thin films prepared by PVD techniques // *Coatings*. 2020, v. 10 (5), p. 447.
9. P. Panjan, M. Čekada, M. Panjan, D. Kek-Merl. Growth defects in PVD hard coatings // *Vacuum*. 2009, v. 84(1), p. 209-214.

Article received 20.02.2025

СТРУКТУРА І ФАЗОВИЙ СКЛАД НАНОЛАМІНАТНИХ ВАКУУМНО-ДУГОВИХ ПОКРИТТІВ ZrTaN/ZrTiCuN

А.В. Таран, І.Є. Гаркуша, В.О. Столбовий, K. Nowakowska-Langier, С.П. Романюк

Досліджено структуру і фазовий склад наноламінатних вакуумно-дугових покриттів ZrTaN/ZrTiCuN. Для вивчення морфології поверхні, хімічного складу та його розподілу використовували спектроскопію комбінаційного розсіювання, скануючу електронну мікроскопію (SEM) з мікроаналізом (EDS), рентгеноструктурний аналіз. Параметри ґратки фаз, виявлених у покриттях за допомогою рентгеноструктурного аналізу, відрізняються від літературних значень, і причиною таких відхилень може бути як наявність макродеформацій у покриттях, так і заміщення цирконію іншими елементами (Ta, Ti, Cu) у підґраткових комірках зазначених вище фаз.